Supporting Material

A Computational Model of Reactive Oxygen Species and Redox Balance in Cardiac Mitochondria

Laura D. Gauthier[‡], Joseph L. Greenstein[‡], Sonia Cortassa[†‡],

Brian O'Rourke[†], and Raimond L. Winslow[‡],

[†]Division of Cardiology, Johns Hopkins University School of Medicine, Baltimore, Maryland, USA
and [‡]Institute for Computational Medicine, Baltimore, Maryland, USA

Methods

Minimal Mitochondrial Model

In order to represent the state-dependent changes in inner membrane potential that occur upon addition of substrate and ADP to substrate-depleted mitochondria, a model of proton leak flux and ATPase were incorporated, based on a previously published model (1) with parameters as given in the supplement. A further addition of a minimal model of ROS scavenging in the mitochondrial matrix, as published in Aon et al. (2) was added to investigate the interplay of ROS production and scavenging.

Computational Methods

The combined ETC model introduced here consists of 14 nonlinear ordinary differential equations describing the oxidation state of 6 Q species on both sides of the membrane, the coupled b_L-b_H redox state, the complex III FeS cluster, cytochrome c_1 and cytochrome c. The equations were implemented in MATLAB 7.1 (The MathWorks, Natick, MA). Model parameters were optimized using the fmincon function from MATLAB. For the protocols described, the model was run until steady-state, when the magnitude of each time derivative was $\leq 10^{-8}$.

Results

Control of Respiration

The activity of the ETC is driven by membrane potential, matrix and cytosolic pH and substrate concentration. Fig. S3 shows the $\Delta\Psi_m$-dependence of model respiration on NADH (Fig. 3A) and succinate (Fig. 3B) compared to experimental data. This dependence follows the characteristic Z-shape (3) with high, saturating respiratory flux for low $\Delta\Psi_m$ decreasing through a linear region for $\Delta\Psi_m$ between state 3 and state 4 values to minimal respiration for $\Delta\Psi_m$ in the high or higher than physiological range. For decreasing ΔpH, expressed as the cytosolic pH less the matrix pH, the V_{O2} vs. $\Delta\Psi_m$ curve shifts leftward (not shown), as in the Magnus and Keizer ETC model(4). Substrate dependence for complex I substrates is validated by comparison with the results of isolated mitochondria undergoing a state 0-4-3 transition protocol. In order the simulate this protocol, the ETC model was expanded into a minimal mitochondrial model with the ability to track changes in $\Delta\Psi_m$ by adding a leak current and a model of the mitochondrial F_O-F_1 ATPase, as previously published (1). The experimental protocol of Wei et al. (1) (their Fig. 4) was simulated in Fig. S4 in the Supporting Material by adjusting NADH levels according to values measured in that experiment and by varying ADP levels accordingly. Model $\Delta\Psi_m$ for all three states is in good agreement with the experimental data from guinea pig cardiac mitochondria, demonstrating appropriate control of model respiration by $\Delta\Psi_m$ and NADH levels.

Supplemental Figures

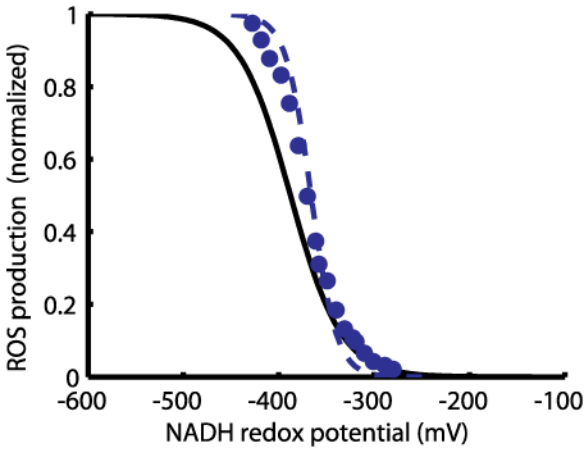

FIGURE S1 Redox potential dependence of complex I-derived ROS.

ROS production from the isolated complex I model was simulated for a range of NADH redox potentials (*solid line*). These results were compared to experimental data (*circles)* from Pryde and Hirst (8)and their fit (*dashed line*)

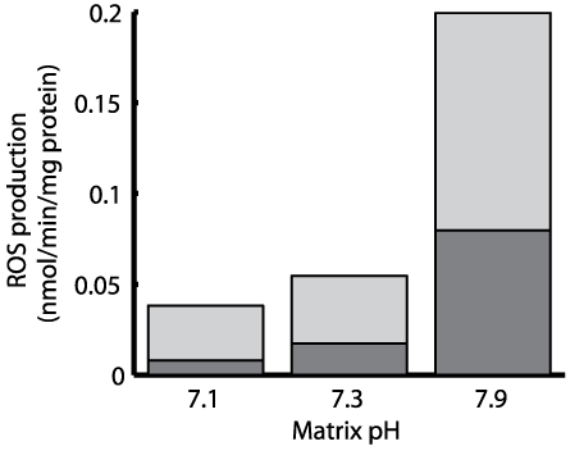

FIGURE S2 Effect of matrix pH on model ROS production under state 4 FET conditions.

ROS production was simulated in glutamate/malate (G/M) in the absence of ADP. Bottom bars (*dark gray)* depict ROS production originating from complex I, top bars (*light gray)* depict matrix-side ROS from complex III. pH 7.3 is representative of the control pH used in other simulations.

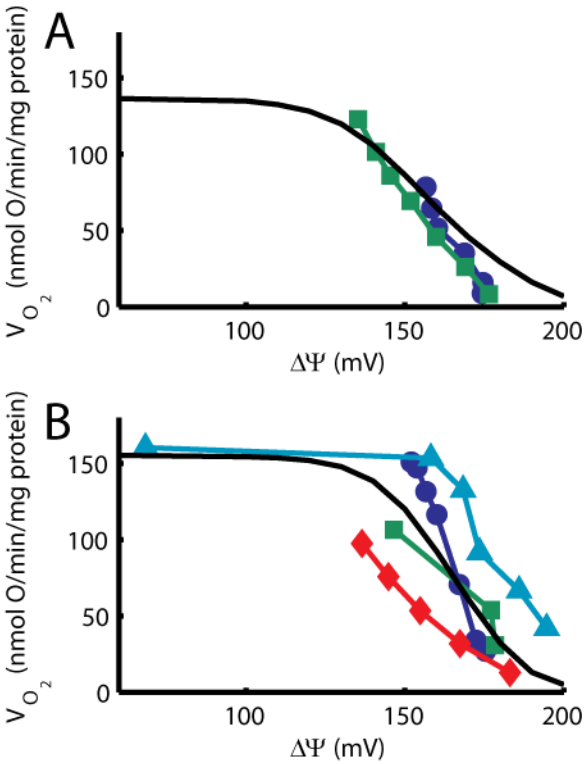

FIGURE S3 $\Delta\Psi_m$-dependence of respiratory rate on complex I and complex II substrates.
(*A)* Model results (*black*) follow closely the experimental measurements from Marcinkeviciute (5) (*circles*) and Lionetti et al. (6) (*squares*), both recorded from isolated mitochondria respiring on glutamate and malate. (*B*) Model simulations (*black*) of mitochondrial respiration on succinate compared with experimental data reproduced from Marcinkeviciute et al. (5) (*circles*) and Lionetti et al. (6) (*squares*), Hafner et al. (7) (*diamonds*), and Murphy and Brand (*triangles*).

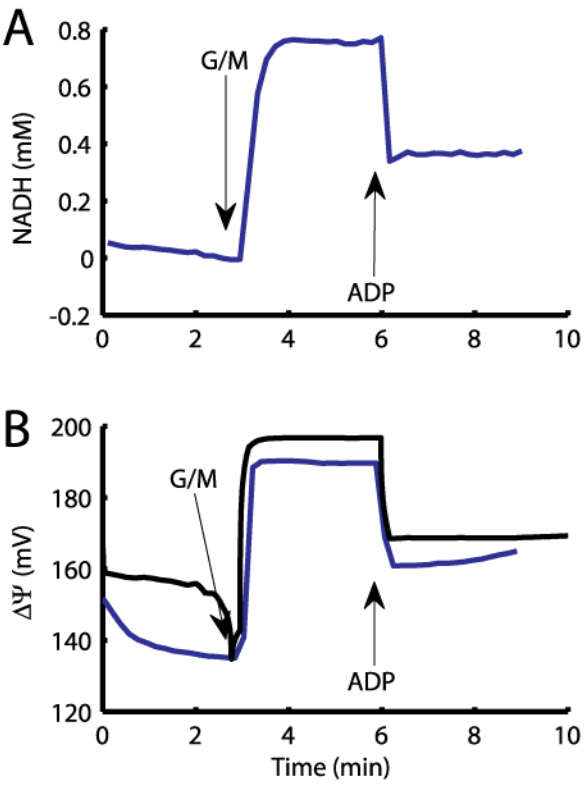

FIGURE S4 Mitochondrial respiratory state transitions.

(*A*) Experimental NADH recordings from Wei et al. (1) in isolated guinea pig heart mitochondria. These data were used as input to the model to simulate a protocol of metabolic transitions from state 1 to state 4 (addition of substrate glutamate/malate) to state 3 (addition of ADP). (*B*) Model $\Delta\Psi_m$ (*black*) closely follows the corresponding experimental measurements (1) of membrane potential (*blue*).

Discussion

Comparison to Existing Models

Computational models must compromise between highly detailed, mechanistic descriptions that are computationally intensive and more phenomenological representations that are more tractable. The model presented here was built while trying to minimize the number of state variables. However, several more detailed models of the ETC exist. The extension of the 1998 Demin model upon which the complex IV model included here was based describes the complete redox state of complex III (b_L, b_H, FeS and cytochrome c_1) and adds the restriction that the semiquinone at the Q_O site does not freely diffuse, but remains localized to the Q_O binding pocket. While this adds more mechanistic detail, it also increases the minimal number of states required to describe the complex III redox state from 3 to 12. This more realistic description of the semiquinone may better reflect the quantitative details of ROS production, but the simplified model used here successfully reproduces the experimentally demonstrated effect of $\Delta\Psi_m$ on complex III ROS production with less computational cost. A series of models has been published by Selivanov et al. (8-10) featuring a highly detailed description of electron transfer and utilizing an innovative algorithm to automate the construction of the ODEs describing the model's redox states. The detailed description of protein redox states in the group's modeling including complex I (9, 10) offers unique insight into the feasibility of the semiquinone-derived complex I ROS production theory. However the 10 states describing complex I and 400 states describing complex III likely preclude the incorporation of this model in its present form into a full mitochondrial model. Orii and Miki (11) published another detailed complex III model including 56 redox states of the enzyme. This model captures to a high degree the complex kinetics the authors observed in their spectrophotometric studies. The combined results of their experimental and modeling studies offer interesting insights into the electron bifurcation between the FeS and b_L redox centers. However, their kinetic studies span durations of three seconds or less. Simulations of metabolic state transitions, during which NADH levels reach steady-state over the course of minutes, might pose a prohibitive computational challenge for this model. More generalized models of the ETC have also been published by Magnus and Keizer(4) and Jin and Bethke(12). The former is the basis for the complex I model included here. The equations describing the various states of the lumped respiratory chain in the Magnus and Keizer ETC model(4) are algebraic, making it an excellent choice for incorporation into integrated models, such as the 2003 mitochondrial energetics model of Cortassa et al. (13) However, because the Magnus and Keizer model (4) is built on a description similar to the ETC supercomplex (14), the model does not include descriptions of the electron carrier intermediates ubiqunone/ubiquinol and cytochrome c. Thus the Cortassa et al. model (13) does not allow determination of ROS production. Jin and Bethke(12) published a more recent ETC model built on a similar non-equilibrium thermodynamics foundation. Theirs is more generalized, allowing for the simulation of respiration on any combination of complex I and complex II substrates, as described by the redox potential of the NAD^+/NADH and succinate/fumarate couples. However, it would be equally difficult to augment this model with an expression for mechanistic ROS production. The mitochondrial and cellular models of ROS-induced ROS release (RIRR) by Cortassa et al. (15) and Zhou et

al. (16), respectively, contain an ad hoc "shunt" description of ROS release as a constant proportion of respiratory flux. As is shown in Fig. 7, there are conditions under which ROS production increases with increases in $\Delta\Psi_m$ and thus follows the opposite trend of respiratory flux. As such, the shunt model cannot account for the control of ROS production in all scenarios. The incorporation of a more mechanistic ETC model, such as the one presented here, will lead to a more complete description of the ROS production component of the RIRR phenomenon.

Modeling Methods

Model code is available online at http://icm.jhu.edu/models.

Section 1. NADH-Ubiquinone Oxidoreductase (Complex I)

A model of complex I was constructed based on the non-equilibrium thermodynamic description from Magnus and Keizer's mitochondrial model(4). To separate the complex I contribution from their lumped ETC model, a state was added in order to incorporate the reduction of Q to QH_2 as the product of complex I. Rate constants were modified from Magnus and Keizer(4) to (roughly) reflect the overall equilibrium constant for the complex I reaction as reported by Chen et al(17). Proton stoichiometry coefficients were reduced to account for the number of protons pumped by complex I only. Proton slip and reaction slip reactions were removed such that oxidation of NADH is completely coupled to proton pumping in the current model. To reduce the state space of the model, Magnus and Keizer represented only the transfer of one electron at a time from NADH. A similar approach was taken here such that the overall reaction is

$$\frac{1}{2}NADH + \frac{1}{2}Q + \frac{1}{2}H^+ + 2H_n^+ \leftrightarrow \frac{1}{2}NAD^+ + \frac{1}{2}QH_2 + 2H_p^+$$

The rate of production of ubiquinol is then twice the flux through the complex I model. To model ROS production from complex I, a reversible reaction between states 4 and 2 was added to represent the transfer of an electron from a reduced redox center in the matrix localized arm of the protein to oxygen according to the widely-accepted model of complex I-derived ROS (18-20). Fig. 1 *B* in the main text gives an overview of the reactions represented in the complex I model. The MATLAB tool KA Pattern (21) was applied to the complex I model in order to derive an algebraic expression for the steady-state electron transfer flux through the complex. Complex I rate constants were optimized using respiratory flux and ROS production rates from Aon et al. (22) as well as NAD^+/NADH and Q/QH_2 redox data from Muraoka and Slater (23).

Rate equations used in complex I model

$a_{12} = a_{12}^* \cdot H_m^2$

$a_{65} = a_{65}^* \cdot H_i^2$

$a_{61} = a_{61}^{*} \cdot \exp(-2 \cdot 0.5 \cdot (\Delta\Psi - \Delta\Psi_B) \cdot F/(RT))$
$a_{16} = a_{16}^{*} \cdot \exp(2 \cdot 0.5 \cdot (\Delta\Psi - \Delta\Psi_B) \cdot F/(RT))$

$a_{23} = a_{23}^{*} NADH^{1/2}$

$a_{43} = a_{43}^{*} (NAD^{+})^{1/2}$

$a_{47} = a_{47}^{*} Q^{1/2} \cdot H_m^{1/2} \cdot (1 - \text{rotenoneBlock})$
where the other half proton is retained from ½NADH

$a_{57} = a_{57}^{*} \cdot (QH_2)^{1/2} \cdot (1 - \text{rotenoneBlock})$

$KeqROS = \exp(2*(E_{O2.-} - E_{FMN}) \cdot F/(RT))$
$a_{42} = a_{42}^{*} \cdot O_2$
$a_{24} = a42 \cdot KeqROS \cdot O_2^{\cdot -}$

$D = E_1 + E_2 + E_3 + E_4 + E_5 + E_6 + E_7$
Numerator terms E1 through E7 have 40 terms, each the product of 6 rate constants. For details, see model code available online at http://www.icm.jhu.edu/models.

$F_1 = E_1/D$
$F_2 = E_2/D$
$F_3 = E_3/D$
$F_4 = E_4/D$
$F_5 = E_5/D$
$F_6 = E_6/D$
$F_7 = E_7/D$

Jres is the steady-state flux of a single electron through complex I in electrons/min
$Jres = 60*\rho_{C1}*(F_4 \cdot a_{47} - F_7 \cdot a_{74})$

v_{c1} is the rate of reduction of Q to QH_2 by complex I, which requires two electrons
$v_{c1} = Jres/2$

$VROS_{c1}$ is the rate of reduction of O_2 to $O_2^{\cdot -}$ by complex I in mM $O_2^{\cdot -}$/min
$VROS_{c1} = 60* \rho_{C1}*(F_4 \cdot a_{42} - F_2 \cdot a_{24})$

TABLE S1. Parameters used in complex I model

Parameter	Description	Value	Reference
ρ_{C1}	concentration of complex I	8.8490mM	fit using data from (22)
$\Delta\Psi_B$	phase boundary potential	50mV	(4)
a_{12}^{*}		$6.3396 \cdot 10^{11}$ $mM^{-2}s^{-1}$	fit using data from (22)
a_{21}		5 s^{-1}	(4)

a_{56}		$100\ s^{-1}$	(4)
a_{65}^{*}		$2.5119 \cdot 10^{13}\ mM^{-2}s^{-1}$	fit using data from (22)
a_{61}^{*}		$10^{7}\ s^{-1}$	fit using data from (22)
a_{16}^{*}		$130\ s^{-1}$	(4)
a_{23}^{*}		$3.8867 \cdot 10^{3}\ mM^{-1/2}s^{-1}$	fit using data from (22)
a_{32}		$9.1295 \cdot 10^{6}\ s^{-1}$	fit using data from (22)
a_{34}		$639.1364\ s^{-1}$	fit using data from (22)
a_{43}^{*}		$3.2882\ mM^{-1/2}s^{-1}$	fit using data from (22)
a_{47}^{*}		$1.5962 \cdot 10^{7}\ mM^{-1}s^{-1}$	fit using data from (22)
a_{74}		$65.2227\ s^{-1}$	fit using data from (22)
a_{75}		$2.4615 \cdot 10^{4}\ s^{-1}$	fit using data from (22)
a_{57}^{*}		$1.1667 \cdot 10^{3}\ mM^{-1/2}s^{-1}$	fit using data from (22)
E_{FMN}	Midpoint potential of flavin mononucleotide	-0.375mV	(24)
$E_{O2.-}$	Midpoint potential of superoxide	-0.15mV	(25)
a_{42}^{*}		$6.0318\ mM^{-1}s^{-1}$	fit using data from (22)

Section 2. Succinate Dehydrogenase (Complex II) and Ubiquinone-Cytochrome c Oxidoreductase (Complex III)

A simplified model of the complex II enzyme was adapted from Demin et al (25). The complex II model represents saturating succinate concentrations and depends only on the ratio of ubiquinol to ubiquinone on the matrix face of the inner membrane. Conditions of varying succinate concentration were simulated by modulating the maximal reaction rate.

The complex III model used here is derived from the representation in Demin et al (25). Briefly, the ratio of forward and backward rate constants for each reaction, as represented in Fig. 1 *C* of the main text, was defined by experimentally-measured redox potentials as described in Demin et al. (25). Parameters were further constrained by fitting the oxidation state of the redox centers in complex III to experimental data from Kim et al. (26) and Brown and Brand (27).

System of differential equations describing complex III

$dQ_n/dt = v_5 - v_{7\_bLox} - v_{7\_bLred} - v_1$

$dQ^{\cdot-}_n/dt = v_{7\_bLox} + v_{7\_bLred} - v_{8\_bLox} - v_{8\_bLred}$

$d(QH_2)_n/dt = v_{8\_bLox} + v_{8\_bLred} + v_1 - v_2$

$d(QH_2)_p/dt = v_2 - v_3$

$dQ^{\cdot-}_p/dt = v_3 - v_{10} - v_{10b} - v_{4\_bHox} - v_{4\_bHred}$

$dQ_p/dt = v_{10} + v_{10b} + v_{4\_bHox} + v_{4\_bHred} - v_5$

$db1/dt = v_{7\_bLox} + v_{8\_bLox} - v_{4\_bHox}$

$db2/dt = v_{4\_bHox} + v_{7\_bLred} + v_{8\_bLred} - v_6$

$db3/dt = -v_{4\_bHred} + v_6 - v_{7\_bLox} - v_{8\_bLox}$

$db4/dt = v_{4\_bHred} - v_{7\_bLred} - v_{8\_bLred}$

$dFeS_{ox}/dt = v_9 - v_3$

$dcyt\ c1_{ox}/dt = v_{33} - v_9$

$dcyt\ c_{ox}/dt = Ve - v_{33}$

$d\Delta\Psi/dt = (VhRes - Vhu - Vhleak)/C_{mito}$

Where b1 represents the b-heme state where b_L and b_H are both oxidized; b2 is b_L reduced, b_H oxidized; b3 is b_L oxidized, b_H reduced; b4 is both reduced.

Rate equations for complexes II and III

Reaction 1 -- reduction of Q to QH_2

$v_1 = v_{c1} + v_{c2}$

(see v_{c1} above)

$$v_{c2} = \frac{V_{SDH} \cdot Q_n/(Q_n + (QH_2)_n)}{K_m + Q_n/(Q_n + (QH_2)_n)}$$

Reaction 2 -- diffusion of QH_2 across the membrane

$v_2 = k_d \cdot ((QH_2)_n - (QH_2)_p)$

Reaction 3 -- QH_2 to FeS e^- transfer

(Note that this reaction describes the oxidation of QH_2 to QH^+ followed by non-redox dependent dissociation of QH^+ into Q and H^+ such that $\Delta E/\Delta pH = -2.3RT/F$-- see Schafer et al. (28) for details.)

$k_3 = k_{03} \cdot Keq3 \cdot \exp(2.3 \cdot (7 - pH_p))$

$k_{-3} = k_{03}$

$v_3 = k_3 \cdot (QH_2)_p \cdot FeS_{ox} - k_{-3} \cdot Q^{\cdot-}_p \cdot FeS_{red} \cdot (1\text{-myxothiazolBlock})$

Reaction 4 – $Q_p^{\cdot-}$ to b_H e^- transfer

$k_{4\_bHox} = k04 \cdot Keq\_4\_bHox \cdot \exp(-\alpha \cdot \delta_1 \cdot F/(RT) \cdot \Delta\Psi)$

$k_{4\_bHred} = k04 \cdot Keq\_4\_bHred \cdot \exp(-\alpha \cdot \delta_1 \cdot F/(RT) \cdot \Delta\Psi)$

$k_{-4\_bHox} = k04 \cdot \exp(\alpha \cdot (1-\delta_1) \cdot F/(RT) \cdot \Delta\Psi)$

$k_{-4\_bHred} = k04 \cdot \exp(\alpha \cdot (1-\delta_1) \cdot F/(RT) \cdot \Delta\Psi)$

$v_{4\_bHox} = k_{4\_bHox} \cdot Q^{\cdot-}_p \cdot b1 - k_{-4\_bHox} \cdot Q_p \cdot b2;$

$v_{4\_bHred} = k_{4\_bHred} \cdot Q^{\cdot-}_p \cdot b3 - k_{-4\_bHred} \cdot Q_p \cdot b4;$

Reaction 5 – diffusion of Q across the membrane
$v_5 = k_d \cdot (Q_p - Q_n)$

Reaction 6 – b_H to b_L e^- transfer
$k_6 = k06 \cdot Keq\_6 \cdot \exp(-\beta \cdot \delta_2 \cdot F/(RT) \cdot \Delta\Psi)$
$k_{-6} = k06 \cdot \exp(\beta \cdot (1-\delta_2) \cdot F/(RT) \cdot \Delta\Psi)$
$v_6 = k_6 \cdot b2 - k_{-6} \cdot b3$

Reaction 7 – b_L to Q_n e^- transfer
$k_{7\_bLox} = k07\_bLox \cdot Keq\_7\_bLox \cdot \exp(-\gamma \cdot \delta_3 \cdot F/(RT) \cdot \Delta\Psi)$
$k_{7\_bLred} = k07\_bLred \cdot Keq\_7\_bLred \cdot \exp(-\gamma \cdot \delta_3 \cdot F/(RT) \cdot \Delta\Psi)$
$k_{-7\_bLox} = k07\_bLox \cdot \exp(\gamma \cdot (1-\delta_3) \cdot F/(RT) \cdot \Delta\Psi)$
$k_{-7\_bLred} = k07\_bLred \cdot \exp(\gamma \cdot (1-\delta_3) \cdot F/(RT) \cdot \Delta\Psi)$
$v_{7\_bLox} = k_{7\_bLox} \cdot Q_n \cdot b3 - k_{-7\_bLox} \cdot Q^{\cdot -}_n \cdot b1 \cdot (1\text{-antimycinBlock})$
$v_{7\_bLred} = k_{7\_bLred} \cdot Q_n \cdot b4 - k_{-7\_bLred} \cdot Q^{\cdot -}_n \cdot b2 \cdot (1\text{-antimycinBlock})$

Reaction 8 -- b_L to $Q_n^{\cdot -}$ e^- and proton transfer
(Note that this reaction describes the reduction of $Q^{\cdot -}$ to QH_2 such that $\Delta E/\Delta pH = -2 \cdot 2.3RT/F$.)
$k_{8\_bLox} = k08\_bLox \cdot Keq\_8\_bLox \cdot \exp(-\gamma \cdot \delta_3 \cdot F/(RT) \cdot \Delta\Psi) \cdot \exp(2.3 \cdot 2 \cdot (7-pH_n))$
$k_{8\_bLred} = k08\_bLred \cdot Keq\_8\_bLred \cdot \exp(-\gamma \cdot \delta_3 \cdot F/(RT) \cdot \Delta\Psi) \cdot \exp(2.3 \cdot 2 \cdot (7-pH_n))$
$k_{-8\_bLox} = k08\_bLox \cdot \exp(\gamma \cdot (1-\delta_3) \cdot F/(RT) \cdot \Delta\Psi)$
$k_{-8\_bLred} = k08\_bLred \cdot \exp(\gamma \cdot (1-\delta_3) \cdot F/(RT) \cdot \Delta\Psi)$
$v_{8\_bLox} = k_{8\_bLox} \cdot Q^{\cdot -}_n \cdot b3 - k_{-8\_bLox} \cdot (QH2)_n \cdot b1 \cdot (1\text{-antimycinBlock})$
$v_{8\_bLred} = k_{8\_bLred} \cdot Q^{\cdot -}_n \cdot b4 - k_{-8\_bLred} \cdot (QH_2)_n \cdot b2 \cdot (1\text{-antimycinBlock})$

Reaction 9 – FeS to cyt c_1 e^- transfer
$k_9 = k09 \cdot Keq9$
$k_{-9} = k09$
$v_9 = k_9 \cdot FeS_{red} \cdot \text{cyt } c1_{ox} - k_{-9} \cdot FeS_{ox} \cdot \text{cyt } c1_{red}$

Reaction 10 – superoxide production from $Q_p^{\cdot -}$
$k_{10} = k010 \cdot Keq10$
$k_{-10} = k010$
$v_{10} = k_{10} \cdot Q^{\cdot -}_p \cdot O_2 - k_{-10} \cdot Q_p \cdot O_2^{\cdot -}$
$v_{10b} = k_{10} \cdot Q^{\cdot -}_p \cdot O_2 - k_{-10} \cdot Q_p \cdot O_2^{\cdot -}$

Reaction 33 – cyt c_1 to cyt c e^- transfer
$v_{33} = k_{33} \cdot \text{cyt } c1_{red} \cdot \text{cyt } c_{ox} - k_{-33} \cdot \text{cyt } c1_{ox} \cdot \text{cyt } c_{red}$

Conservation relations
$FeS_{red} = c3_{tot} - FeS_{ox}$
$\text{cyt } c1_{red} = c3_{tot} - \text{cyt } c1_{ox}$
$\text{cyt } c_{red} = \text{cyt } c_{tot} - \text{cyt } c_{ox}$

TABLE S2. Parameters used in the complexes II and III models

Parameter	Description	Value	Reference
Vsucc	Maximum velocity of SDH	250 mM/min	fit using data from (26)
Km_succ	Michaelis constant for SDH	0.6	(25)
k03	Reverse rate constant for reaction 3	$9.9998 \cdot 10^4$	fit using data from (26)
Keq3	Equilibrium constant for reaction 3	0.6877	(25)
k04	Reverse rate constant for reaction 3	$3.6402 \cdot 10^3$	fit using data from (26)
Keq4_bHox	Equilibrium constant for reaction 4 (b_H oxidized)	129.9853	fit using data from (26)
Keq4_bHred	Equilibrium constant for reaction 4 (b_H reduced)	13.7484	fit using data from (26)
δ_1	Fraction of $\Delta\Psi$ at energy barrier peak for reaction 4	0.5	(25)
α	Fraction of $\Delta\Psi$ affecting $Q_p^{\cdot-}$ to b_L e^- transfer	0.2497	Derived from β value, assuming membrane symmetry
k_d	Rate of diffusion across the membrane for Q and QH_2	$1.32 \cdot 10^6$ /min	(25)
k06	Reverse rate constant for reaction 6	10,000	fit using data from (26)
Keq6	Equilibrium constant for reaction 6	9.4546	fit using data from (26)
δ_2	Fraction of $\Delta\Psi$ at energy barrier peak for reaction 6	0.5	(25)
β	Fraction of $\Delta\Psi$ affecting b_L to b_H e^- transfer	0.5006	fit using data from (26)
k07_bLox	Reverse rate constant for reaction 7 (b_L oxidized)	800	fit using data from (26)
Keq7_bLox	Equilibrium constant for reaction 7 (b_L oxidized)	3.0748	(25)
k07_bLred	Reverse rate constant for reaction 7 (b_L reduced)	100	fit using data from (26)

Keq7_bLred	Equilibrium constant for reaction 7 (b_L reduced)	29.0714	Adjusted from (25) by for anticooperativity as given in (26)
δ_3	Fraction of $\Delta\Psi$ at energy barrier peak for reaction 7	0.5	(25)
γ	Fraction of $\Delta\Psi$ affecting b_H to Q_n e^- transfer	0.2497	Derived from β value, assuming membrane symmetry
k08_bLox	Reverse rate constant for reaction 8 (b_L oxidized)	5000	fit using data from (26)
Keq8_bLox	Equilibrium constant for reaction 8 (b_L oxidized)	129.9853	(26)
k08_bLred	Reverse rate constant for reaction 8 (b_L oxidized)	500	fit using data from (26)
Keq8_bLred	Equilibrium constant for reaction 8 (b_L reduced)	9.4546	(26)
k09	Reverse rate constant for reaction 9	$4.9949 \cdot 10^4$	fit using data from (26)
Keq9	Equilibrium constant for reaction 9	0.2697	(25)
k010	Reverse rate constant for reaction 10	50	fit using data from (26)
Keq10	Equilibrium constant for reaction 10	1.4541	(26)
k33		148,148	(29)
Keq33	Equilibrium constant for reaction 33	2.1145	(26)
C3tot	Total complex III protein	0.325mM	(29)

Equilibrium constants were adjusted to 37°C

Section 3. Cytochrome c Oxidase (Complex IV)

The complex IV model used here is derived from the representation in Demin et al.(29) as depicted in Fig. 1 *D* of the main text. Model parameters were refit to match data on $\Delta\Psi_m$-dependence of oxygen consumption (5) and cytochrome c redox state (26, 27) The binding affinity for oxygen was set according to measurements by Brzezinski and Adelroth (30). KA Pattern (21) was also applied to this model to derive an algebraic expression for oxygen consumption.

Rate constants of complex II, III and IV reactions were optimized to fit the data shown in Figs. 2-4 from ref. (26) while maintaining the equilibrium constants as determined by redox potentials from the literature. Complex I rate constants were optimized to fit data from ref. (22), as presented in Fig. 7. Experimental data from cardiac mitochondria were used whenever possible.

Rate equations used in complex IV model

$$a_{12} = k_{34} \cdot \exp(-d_5 \cdot 4 \cdot \Delta\Psi \frac{F}{RT}) \cdot cytc_{red}{}^3 \cdot H_n{}^4$$

$$a_{14} = k_{-37} \cdot \exp((1-d_5) \cdot \Delta\Psi \frac{F}{RT}) \cdot H_p$$

$$a_{21} = k_{-34} \cdot \exp((1-d_5) \cdot 4 \cdot \Delta\Psi \frac{F}{RT}) \cdot cytc_{ox}{}^3 \cdot H_p$$

$$a_{23} = k_{35} \cdot O_2 \cdot (1 - CNBlock)$$

$$a_{34} = k_{36} \cdot \exp(-d_5 \cdot 3 \cdot \Delta\Psi \frac{F}{RT}) \cdot cytc_{red} \cdot H_n{}^3$$

$$a_{41} = k_{37} \cdot \exp(-d_5 \cdot \Delta\Psi \frac{F}{RT}) \cdot H_n$$

$$a_{43} = k_{-36} \cdot \exp((1-d_5) \cdot 3 \cdot \Delta\Psi \frac{F}{RT}) \cdot cytc_{ox} \cdot H_p{}^2$$

$E_1 = a_{21} \cdot a_{41} \cdot a_{34} + a_{41} \cdot a_{34} \cdot a_{23}$
$E_2 = a_{12} \cdot a_{41} \cdot a_{34}$
$E_3 = a_{23} \cdot a_{12} \cdot a_{41} + a_{43} \cdot a_{14} \cdot a_{21} + a_{23} \cdot a_{43} \cdot a_{12} + a_{23} \cdot a_{43} \cdot a_{14}$
$E_4 = a_{14} \cdot a_{34} \cdot a_{21} + a_{34} \cdot a_{23} \cdot a_{12} + a_{14} \cdot a_{34} \cdot a_{23}$

$D = E_1 + E_2 + E_3 + E_4$

$Y = E_1/D$
$Yr = E_2/D$
$YO = E_3/D$
$YOH = E_4/D$

$v_{34} = C4_{tot} \cdot (Y \cdot a_{12} - Yr \cdot a_{21})$
$v_{35} = C4_{tot} \cdot Yr \cdot a_{23}$
$v_{36} = C4_{tot} \cdot (a_{34} \cdot YO - a_{43} \cdot YOH)$
$v_{37} = C4_{tot} \cdot (a_{41} \cdot YOH - a_{14} \cdot Y)$

$V_e = 3v_{34} + v_{35}$
$V_H = 4v_{34} + 3v_{36} + v_{37}$
$V_{O2} = v_{35}$

$VhRes = 2v_3 + V_H$

TABLE S3. Parameters used in complex IV model

Parameter	Description	Value	Reference
cyt c_{tot}	Total cytochrome c	0.325mM	(29)
$C4_{tot}$	Total complex IV protein	0.325mM	(29)
k_{34}		$1.7667 \cdot 10^{28}$	Adjusted from (29) to fit (26)
k_{-34}		1.7402	Adjusted from (29) to fit (26)
k_{35}		45,000	(30)
k_{36}		$2.8955 \cdot 10^{25}$	Adjusted from (29) to fit (26)
k_{-36}		$2.8955 \cdot 10^{10}$	Adjusted from (29) to fit (26)
k_{37}		$1.7542 \cdot 10^{12}$	Adjusted from (29) to fit (26)
k_{-37}		$1.7542 \cdot 10^{4}$	Adjusted from (29) to fit (26)
δ_5		0.5	(29)
O_2	Matrix oxygen concentration	$6 \cdot 10^{-3}$mM	(29)
$O_2^{\cdot -}$	Matrix superoxide concentration	$0.1 \cdot 10^{-3}$mM	(29)

Section 4. ATP generation and proton leak systems

$\Delta pH = pH_p - pH_n$

$\mu_H = -2.303 \cdot RT/F \cdot \Delta pH + \Delta\Psi$

$$V_{AF1} = \frac{K_{ATPase\_app} \cdot ATP}{P_i \cdot (ADP^{3+} + HADP)}$$

$$Vhu = -\rho_{F1} \frac{300 \cdot p_a + 300 \cdot p_a \cdot V_{AF1} - 3e^{3\frac{F}{RT}\mu_H}(p_a + p_b)}{e^{150\frac{F}{RT}} + p_1 \cdot e^{150\frac{F}{RT}} \cdot V_{AF1} + e^{3\frac{F}{RT}\mu_H}(p_2 + p_3 * V_{AF1})}$$

$Vhleak = gH \cdot \mu_H$

TABLE S4. Parameters for ATP generation and proton leak systems

Parameter	Description	Value	Reference
C_{mito}	mitochondrial membrane capacitance	$1.812 \cdot 10^{-3}$mM/mV	(1)
K_{ATPase_app}	Apparent equilibrium constant for ATPase	$4.1175 \cdot 10^{6}$	
Pi	total concentration of inorganic phosphate	8.6512mM	
HADP	concentration of proton-bound ATP	0.0026mM	
ρ_{F1}	concentration of ATPase	5mM	
p_a		$9.936 \cdot 10^{-4}$ min^{-1}	(4)
p_b		$2.0238 \cdot 10^{-5}$ min^{-1}	(4)
p_1		$1.346 \cdot 10^{-4}$	(4)
p_2		$7.739 \cdot 10^{-7}$	(4)
p_3		$6.65 \cdot 10^{-15}$	(4)

Section 5. Simulation Settings

Inputs to the model (with the exception of Fig.10) are cytosolic pH (pH_p), matrix pH (pH_n), $\Delta\Psi$ (if clamped), NADH, NAD, percent maximal succinate dehydrogenase activity, myxothiazol inhibition, antimycin inhibition, rotenone inhibition, cyanide inhibition, mitochondrial membrane proton leak conductance (gh), matrix ATP, and matrix ADP. Fig. 10 presents results from the isolated complex I model using clamped $\Delta\Psi$ and Q and QH_2 as additional inputs. The values of these inputs for each figure are given in the tables below. Inhibitors are off unless otherwise stated. In the absence of succinate or malate measurements, SDH activity was fit using the data.

TABLE S5. Simulation parameters for Figs. 2A-C

Parameter	Value
pH_p	7.0
pH_n	7.3
$\Delta\Psi$	clamped to values ranging from 70 to 200mV
NADH	1mM
NAD^+	9mM
SDH activity	60%
gh	0.12mM/min/mV
ATP	0.01mM
ADP	0.0110mM

NADH:NAD ratio comes from most reduced estimate by Mintz and Robin (31) for alveolar macrophages to compare to Kim et al. (26) RAW macrophages. SDH activity was increased to fit the Q/QH_2 redox data in accordance with the observation from a previously published mitochondria model (13) that SDH activity is increased as NADH becomes oxidized.

TABLE S6. Simulation parameters for Figs. 3 and 5 *B*

Parameter	Value
pH_p	7.0
pH_n	7.6
gh	0.12mM/min/mV
ATP	0.01mM
ADP	0.0110mM
RET-4 $\Delta\Psi$	195mV
RET-4 NADH	8.168mM
RET-4 NAD^+	1.832mM
RET-4 SDH activity	50%
RET-3 $\Delta\Psi$	150mV
RET-3 NADH	2.560mM
RET-3 NAD^+	7.440mM
RET-3 SDH activity	50%

RET-4 ΔΨ	190mV
FET-4 NADH	3.489mM
FET-4 NAD^+	6.511mM
FET-4 SDH activity	5%
FET-3 ΔΨ	155mV
FET-3 NADH	2.147mM
FET-3 NAD^+	7.853mM
FET-3 SDH activity	5%

ΔΨ values from Aon et al. (22), their figures 3B and C. NAD^+/NADH estimates from Muraoka and Slater (23) 10mM pyruvate protocol. SDH activity for FET simulations was kept low to reproduce the trend of increasingly oxidized Q for RET-4, RET-3, FET-4, followed by FET-3 shown in the pyruvate and succinate data from Muraoka and Slater (23).

TABLE S7. Simulation parameters for Figs. 4 and S3 *B*

Parameter	Value
pH_p	7.0
pH_n	7.6
ΔΨ	clamped to values ranging from 0 to 200mV
NADH	2.3055mM
NAD^+	7.685mM
SDH activity	100%
gh	0.12mM/min/mV
ATP	0.01mM
ADP	0.0110mM
rotenone block	100%

TABLE S8. Simulation parameters for Fig. 5 *A*

Parameter	Value
pH_p	7.2
pH_n	7.3 to 7.8
ΔΨ	200mV
NADH	2.5mM
NAD^+	7.5mM
SDH activity	100%
gh	0.12mM/min/mV
ATP	0.01mM
ADP	0.0110mM

Fig. 5 *B* uses conditions from Fig. 3 with pH_n = {7.6, 8.0, 8.3}

TABLE S9. Simulation parameters for Fig. 6 *A*

Parameter	Value
pH_p	7.0
pH_n	7.6
gh	0.12mM/min/mV

ATP	0.01mM
ADP	0.0110mM
G/M	
NADH	3.489mM
NAD^+	6.511mM
$\Delta\Psi$	unclamped
SDH activity	20%
G/M + rot	
NADH	3.489mM
NAD^+	6.511mM
$\Delta\Psi$	unclamped
SDH activity	20%
rotenone block	95%

NAD^+/NADH estimates from Muraoka and Slater (23) 10mM pyruvate protocol.

TABLE S10. Simulation parameters for Fig. 6 *B*

Parameter	Value
pH_p	7.0
pH_n	7.6
gh	0.12mM/min/mV
ATP	0.01mM
ADP	0.0110mM
succ + rot	
NADH	0mM
NAD^+	10mM
$\Delta\Psi$	unclamped
SDH activity	50%
rotenone block	95%
succ + rot + AA	
NADH	0mM
NAD^+	10mM
$\Delta\Psi$	unclamped
SDH activity	50%
rotenone block	95%
antimycin A block	77.5%
succ + rot + myx	
NADH	0mM
NAD^+	10mM
$\Delta\Psi$	unclamped
SDH activity	50%
rotenone block	95%
myxothiazol block	85%

TABLE S11. Simulation parameters for Fig. 7

Parameter	Value
pH_p	7.0
pH_n	7.6
$\Delta\Psi$	unclamped
NADH	3mM
NAD^+	7mM
SDH activity	20%
gh	varied from 0.12 to 8.4 mM/min/mV
ATP	0.01mM
ADP	0.0110mM

TABLE S12. Simulation parameters for Fig. S1

Parameter	Value
pH_p	7.0
pH_n	7.5
$\Delta\Psi$	129.2445mV
NADH	0.03mM
NAD^+	ranges from 10^{-10} to 10^{-5}mM
Q	0mM
QH_2	0mM
rotenone block	100%

TABLE S13. Simulation parameters for Fig. S2

Parameter	Value
pH_p	7.0
pH_n	7.1, 7.3, 7.9
$\Delta\Psi$	200mV
NADH	3.489mM
NAD^+	6.511mM
SDH activity	5%
gh	0.12mM/min/mV
ATP	0.01mM
ADP	0.0110mM

TABLE S14. Simulation parameters for Fig. S3 *A*

Parameter	Value
pH_p	7.0
pH_n	7.6
$\Delta\Psi$	clamped to values ranging from 0 to 200mV
NADH	2.3055mM
NAD^+	7.685mM

SDH activity	20%
gh	0.12mM/min/mV
ATP	0.01mM
ADP	0.0110mM

Fig. S3B uses the same settings as Fig. 4

TABLE S15. Simulation parameters for Fig. S4

Parameter	Value
pH_p	7.0
pH_n	7.3
$\Delta\Psi$	unclamped
SDH activity	20%
gh	0.12mM/min/mV
NADH	Wei et al. recordings, their figure 4D
NAD^+	10-NADH
state 0 ATP	0.01mM
state 0 ADP	0.0110mM
state 4 ATP	1.2223mM
state 4 ADP	0.0110mM
state 3 ATP	1.2223mM
state 3 ADP	1.0mM

Section 6. Minimal scavenging model

Equations and parameters are reproduced from the code for simulations in Aon et al. (2).

System of differential equations describing ROS scavenging

$d[H_2O_2]/dt = V_{SOD} - k_1 \cdot [H_2O_2] - V_{Prx} - V_{Gpx}$
$d[GSH]/dt = V_{GR} - V_{GPx}$
$d[Trx(SH)_2]/dt = V_{TrxR} - V_{TxPx}$
$d[Prx(SH)_2]/dt = V_{TxPx} - V_{Prx}$

Rate equations for ROS scavenging

Rate of glutathione peroxidase (GPx), oxidizes GSH, detoxifies H_2O_2

$$V_{GPx} = \frac{E_T^{GPx}[H_2O_2][GSH]}{\Phi_1[GSH] + \Phi_2[H_2O_2]}$$

Rate of glutathione reductase (GR), reduces GSSG to 2GSH

$$V_{GR} = \frac{k_{GR} E_T^{GR}[GSSG][NADPH]}{[GSSG][NADPH] + K_M^{GSSG}[NADPH] + K_M^{NADPH}[GSSG] + K_M^{GSSG} K_M^{NADPH}}$$

Rate of peroxiredoxin (a.k.a. thioredoxin-dependent peroxidase) oxidation, detoxifies H_2O_2

$$V_{Prx} = \frac{E_T^{Prx}[H_2O_2][Prx(SH)_2]^2}{\Phi_{P2}[Prx(SH)_2] + \Phi_{P1}[H_2O_2]}$$

Rate of thioredoxin reductase (TrxR)

$$V_{TrxR} = \frac{k_{TrxR} E_T^{TrxR}[Trx(SS)][NADPH]}{[Trx(SS)][NADPH] + K_M^{Trx(SS)}[NADPH] + K_M^{T\text{-}NADPH}[Trx(SS)] + K_M^{Trx(SS)} K_M^{T\text{-}NADPH}}$$

Rate of peroxidredoxin reduction and thioredoxin oxidation

$$V_{TxPx} = k_{TxPx}[Trx(SH)_2][Prx(SS)]$$

Conservation relations

$GSSG = 0.5 \cdot (G_{tot} - GSH)$
$Trx(SS) = Trx_{tot} - Trx(SH)_2$
$Prx(SS) = Prx_{tot} - Prx(SH)_2$

TABLE S16. Parameters for scavenging model

Parameter	Description	Value
E_T^{GPX}	concentration of GPx	0.0034mM
Φ_1	GPx activity constant	$1.1337 \cdot 10^{-7}$/min
Φ_2	GPx activity constant	$2.5 \cdot 10^{-5}$/min
E_T^{GR}	concentration of GR	$5 \cdot 10^{-3}$mM
k_{GR}	rate constant of GR	1500/min

K_M^{GSSG}	K_M of GR for oxidized GSH	0.12mM
K_M^{NADPH}	K_M of GR for NADPH	0.015mM
G_{tot}	total glutathione pool	3mM
E_T^{Prx}	concentration of Prx	1mM
Φ_{P1}	Prx activity constant	$6.3833 \cdot 10^{-6}$/min
Φ_{P2}	Prx activity constant	$3.0833 \cdot 10^{-7}$/min
$K_M^{Trx(SS)}$	K_M of TrxR for Trx(SS)	0.006
$K_M^{T\text{-}NADPH}$	K_M of TrxR for NADPH	0.012
k_{TrxR}	rate constant of TrxR	$1.32 \cdot 10^{3}$/min
E_T^{TrxR}	concentration of TrxR	0.01
k_{TxPx}	rate constant of Prx	$1.5 \cdot 10^{5}$/min
Trx_{tot}	total thioredoxin pool	0.025
Prx_{tot}	total peroxiredoxin pool	0.15
k_1	rate constant of H_2O_2 transport from mitochondria	0.002

Section 7. Initial conditions

TABLE S17. Initial conditions

State variable	Value
Q_n	1.2518 mM
$Q^{\cdot -}_n$	0.5578 mM
$(QH_2)_n$	0.4199 mM
$(QH_2)_p$	0.4197 mM
$Q^{\cdot -}_p$	0.0988 mM
Q_p	1.2520 mM
b1	0.0618 mM
b2	0.1500 mM
b3	0.0954 mM
b4	0.0179 mM
FeS_{ox}	0.0900 mM
FeS_{red}	0.2350 mM
cyt $c1_{ox}$	0.2266 mM
cyt c_{ox}	0.1785 mM
cyt $c1_{red}$	0.0984 mM
cyt c_{red}	0.1465 mM
$\Delta\Psi$ (only relevant if unclamped)	180mV
H_2O_2 (only with scavenging model)	0 mM
GSH (only with scavenging model)	2.8 mM
$Trx(SH)_2$ (only with scavenging model)	0.002 mM
$Prx(SH)_2$ (only with scavenging model)	0.0281 mM

Supporting References

1. Wei, A.-C., Miguel A. Aon, B. O'Rourke, Raimond L. Winslow, and S. Cortassa. 2011. Mitochondrial Energetics, pH Regulation, and Ion Dynamics: A Computational-Experimental Approach. Biophysical journal 100:2894-2903.
2. Aon, M. A., B. A. Stanley, V. Sivakumaran, J. M. Kembro, B. O'Rourke, N. Paolocci, and S. Cortassa. 2012. Glutathione/thioredoxin systems modulate mitochondrial H2O2 emission: An experimental-computational study. The Journal of General Physiology 139:479-491.
3. Pietrobon, D., and S. R. Caplan. 1985. Flow-force relationships for a six-state proton pump model: intrinsic uncoupling, kinetic equivalence of input and output forces, and domain of approximate linearity. Biochemistry 24:5764-5776.
4. Magnus, G., and J. Keizer. 1997. Minimal model of beta-cell mitochondrial Ca2+ handling. American Journal of Physiology - Cell Physiology 273:C717-C733.
5. Marcinkeviciute, A., V. Mildaziene, S. Crumm, O. Demin, J. B. Hoek, and B. Kholodenko. 2000. Kinetics and control of oxidative phosphorylation in rat liver mitochondria after chronic ethanol feeding. The Biochemical journal 349:519-526.

6. Lionetti, L., S. Iossa, M. D. Brand, and G. Liverini. 1996. Relationship between membrane potential and respiration rate in isolated liver mitochondria from rats fed an energy dense diet. Molecular and Cellular Biochemistry 158:133-138.
7. Hafner, R. P., G. C. Brown, and M. D. Brand. 1990. Analysis of the control of respiration rate, phosphorylation rate, proton leak rate and protonmotive force in isolated mitochondria using the 'top-down' approach of metabolic control theory. European Journal of Biochemistry 188:313-319.
8. Selivanov, V. A., T. V. Votyakova, J. A. Zeak, M. Trucco, J. Roca, and M. Cascante. 2009. Bistability of Mitochondrial Respiration Underlies Paradoxical Reactive Oxygen Species Generation Induced by Anoxia. PLoS Comput Biol 5:e1000619.
9. Selivanov, V. A., T. V. Votyakova, V. N. Pivtoraiko, J. Zeak, T. Sukhomlin, M. Trucco, J. Roca, and M. Cascante. 2011. Reactive Oxygen Species Production by Forward and Reverse Electron Fluxes in the Mitochondrial Respiratory Chain. PLoS Comput Biol 7:e1001115.
10. Selivanov, V. A., M. Cascante, M. Friedman, M. F. Schumaker, M. Trucco, and T. V. Votyakova. 2012. Multistationary and Oscillatory Modes of Free Radicals Generation by the Mitochondrial Respiratory Chain Revealed by a Bifurcation Analysis. PLoS Comput Biol 8:e1002700.
11. Orii, Y., and T. Miki. 1997. Oxidation Process of Bovine Heart Ubiquinol-Cytochrome c Reductase as Studied by Stopped-flow Rapid-scan Spectrophotometry and Simulations Based on the Mechanistic Q Cycle Model. Journal of Biological Chemistry 272:17594-17604.
12. Jin, Q., and C. M. Bethke. 2002. Kinetics of Electron Transfer through the Respiratory Chain. Biophysical Journal 83:1797-1808.
13. Cortassa, S., M. A. Aon, E. Marbán, R. L. Winslow, and B. O'Rourke. 2003. An Integrated Model of Cardiac Mitochondrial Energy Metabolism and Calcium Dynamics. Biophysical journal 84:2734-2755.
14. Lenaz, G., and M. L. Genova. 2007. Kinetics of integrated electron transfer in the mitochondrial respiratory chain: random collisions vs. solid state electron channeling. American Journal of Physiology - Cell Physiology 292:C1221-C1239.
15. Cortassa, S., M. A. Aon, R. L. Winslow, and B. O'Rourke. 2004. A Mitochondrial Oscillator Dependent on Reactive Oxygen Species. Biophysical Journal 87:2060-2073.
16. Zhou, L., S. Cortassa, A.-C. Wei, M. A. Aon, R. L. Winslow, and B. O'Rourke. 2009. Modeling Cardiac Action Potential Shortening Driven by Oxidative Stress-Induced Mitochondrial Oscillations in Guinea Pig Cardiomyocytes. Biophysical journal 97:1843-1852.
17. Chen, X., F. Qi, R. K. Dash, and D. A. Beard. 2010. Kinetics and Regulation of Mammalian NADH-Ubiquinone Oxidoreductase (Complex I). Biophysical Journal 99:1426-1436.
18. Kussmaul, L., and J. Hirst. 2006. The mechanism of superoxide production by NADH:ubiquinone oxidoreductase (complex I) from bovine heart mitochondria. PNAS 103:7607-7612.
19. Pryde, K. R., and J. Hirst. 2011. Superoxide Is Produced by the Reduced Flavin in Mitochondrial Complex I. Journal of Biological Chemistry 286:18056-18065.
20. Genova, M. L., B. Ventura, G. Giuliano, C. Bovina, G. Formiggini, G. Parenti Castelli, and G. Lenaz. 2001. The site of production of superoxide radical in mitochondrial Complex I is not a bound ubisemiquinone but presumably iron-sulfur cluster N2. FEBS letters 505:364-368.
21. Qi, F., R. K. Dash, Y. Han, and D. A. Beard. 2009. Generating rate equations for complex enzyme systems by a computer-assisted systematic method. BMC bioinformatics 10:238.
22. Aon, M. A., S. Cortassa, and B. O'Rourke. 2010. Redox-optimized ROS balance: A unifying hypothesis. Biochimica et Biophysica Acta (BBA) - Bioenergetics 1797:865-877.
23. Muraoka, S., and E. C. Slater. 1969. The redox states of respiratory-chain components in rat-liver mitochondria II. The "crossover" on the transition from State 3 to State 4. Biochimica et Biophysica Acta (BBA) - Bioenergetics 180:227-236.

24. Sled, V. D., N. I. Rudnitzky, Y. Hatefi, and T. Ohnishi. 1994. Thermodynamic Analysis of Flavin in Mitochondrial NADH:Ubiquinone Oxidoreductase (Complex I). Biochemistry 33:10069-10075.
25. Demin, O. V., B. N. Kholodenko, and V. P. Skulachev. 1998. A model of O2.- generation in the complex III of the electron transport chain. Molecular and Cellular Biochemistry 184:21-33.
26. Kim, N., M. O. Ripple, and R. Springett. 2012. Measurement of the Mitochondrial Membrane Potential and pH Gradient from the Redox Poise of the Hemes of the bc1 Complex. Biophysical journal 102:1194-1203.
27. Brown, G. C., and M. D. Brand. 1985. Thermodynamic control of electron flux through mitochondrial cytochrome bc1 complex. The Biochemical journal 225:399-405.
28. Schafer, F. Q., and G. R. Buettner. 2001. Redox environment of the cell as viewed through the redox state of the glutathione disulfide/glutathione couple. Free Radical Biology and Medicine 30:1191-1212.
29. Demin, O. V., I. I. Goryanin, B. N. Kholodenko, and H. V. Westerhoff. 2001. Kinetic Modeling of Energy Metabolism and Superoxide Generation in Hepatocyte Mitochondria. Molecular Biology 35:940-949.
30. Brzezinski, P., and P. Ädelroth. 1998. Pathways of Proton Transfer in Cytochrome c Oxidase. Journal of Bioenergetics and Biomembranes 30:99-107.
31. Mintz, S., and E. D. Robin. 1971. Redox state of free nicotinamide-adenine nucleotides in the cytoplasm and mitochondria of alveolar macrophages. J Clin Invest 50:1181-1186.